X- and Q-band magnetic resonance study of iridium-doped silver chloride microcrystals

2000 J. Phys.: Condens. Matter 12 10611

(http://iopscience.iop.org/0953-8984/12/50/321)

J. Phys.: Condens. Matter **12** (2000) 10611–10621. Printed in the UK PII: S0953-8984(00)16230-7

X- and Q-band magnetic resonance study of iridium-doped silver chloride microcrystals

K Sabbe†, H Vrielinck†, F Callens† and D Vandenbroucke‡

† Department of Solid State Sciences, Ghent University, Krijgslaan 281-S1, B-9000 Ghent, Belgium

‡ Agfa-Gevaert Research Laboratories, Septestraat 27, B-2640 Antwerp, Belgium

E-mail: kris.sabbe@rug.ac.be (K Sabbe), henk.vrielink@rug.ac.be (H Vrielinck), freddy.callens@rug.ac.be (F Callens) and dirk.vandenbroucke.dv@belgium.agfa.com (D Vandenbroucke)

Received 8 August 2000, in final form 18 October 2000

Abstract. Irradiation at low temperature ($T < 120$ K) of iridium-doped AgCl microcrystals with x-rays leads to the formation of a single Ir^{2+} complex. The comparison between X- and Q-band EPR (electron paramagnetic resonance) spectra reveals that the defect has a small orthorhombic distortion. Pulse annealing to temperatures higher than 170 K converts the complex into a second Ir^{2+} complex with axial symmetry. This conversion is monitored with X-band ENDOR (electron–nuclear double resonance), allowing a consistent spectrum decomposition and interpretation. For each defect a model is proposed.

1. Introduction

Trivalent transition metal ions are incorporated into AgX (X = Cl, Br) photographic emulsions by coprecipitation from an aqueous solution in order to change the photographic properties. The majority of these doping ions occupy substitutional positions in the cation sublattice and serve as electron or hole traps. Ir^{3+} is widely used in commercial photographic emulsions. The addition of very small quantities can increase the internal sensitivity, reduce fog, reduce high-intensity reciprocity failure, increase the image density or affect the developability of the latent image [1]. It is assumed that changes in the environment of the Ir^{3+} ion, e.g. ligand exchange or the presence of vacancies, can influence the trap depth and the trapping efficiency. Therefore, a detailed microscopic model and knowledge of the decay mechanisms of the iridium defects in AgX is very important. The study of Rh centres in AgX [2–9] has shown that a combination of EPR and ENDOR is ideally suited for such a study.

Ir^{3+} can trap an electron during UV or x-ray irradiation and become Ir^{2+} ($5d^7$), which is paramagnetic and can be studied with EPR or ENDOR. Both techniques are favourably applied to single crystals. Because large AgX single crystals cannot be grown from solution, large melt-grown crystals have been used as model systems. Iridium complexes in AgCl and AgBr single crystals have been studied with EPR and the spectra were assigned to $[IrCl_6]^{4-}$ and $[IrBr_6]^{4-}$ respectively [10, 11]. NaCl single crystals, which can be successfully grown from both the melt and solution, have also been used as model systems. An EPR study on solution-grown NaCl single crystals doped with Ir^{3+} revealed the presence of two axial $[IrCl_6]^{4-}$ defects, but no structural model was proposed [12]. Recently also melt-grown NaCl single crystals doped

0953-8984/00/5010611+11$30.00

with Ir^{3+} were studied with X-band EPR and ENDOR, immediately after x-ray irradiation at 77 K. A single $[IrCl_6]^{4-}$ complex was observed [13], different from both axial centres in solution-grown NaCl single crystals. For all of these Ir^{2+} ($5d^7$) centres in NaCl and AgX the general EPR and ENDOR parameters, i.e. the g-tensor, iridium hyperfine interaction (EPR) and the strong interaction with two axial chlorine or bromine nuclei (EPR and ENDOR) and the two axial sodium nuclei (ENDOR) [10–13], are well understood.

The present study reports the results of EPR and ENDOR experiments on the iridium centres formed in iridium-doped AgCl photographic emulsions after x-ray irradiation at low temperature ($T < 120$ K) and subsequent pulse annealing. Because the photographic consequences of doping depend on the nature of the trapped centres and their precursors, their stability and the reactions that follow the exposure, an attempt will be made to find an answer to these questions for the iridium centres in AgCl.

2. Materials and methods

Cubic AgCl microcrystals doped with 50 ppm of iridium were grown using the double-jet precipitation method. The dopant salt was $Na_2IrCl_6{\cdot}6H_2O$. The photographic emulsions were grown in a gelatin solution at relatively high pH and high pAg, yielding a weakly reducing medium. The result is that the Ir^{4+} is very rapidly reduced to Ir^{3+} even before incorporation into the AgX matrix. This fast reduction was confirmed by spectrophotometric measurements in gelatin solutions and by EPR measurements on Ir^{4+}-doped silver halides before exposure. The emulsions were enzymatically degelled and dried to obtain a powder suitable for EPR and ENDOR measurements.

The AgCl powders were x-ray irradiated for typically 30 minutes with a tungsten anticathode x-ray tube (Philips) operated at 60 kV and 40 mA. During x-ray irradiation the powder was put on a metal surface in contact with liquid nitrogen (77 K). Afterwards the powder was transferred to a liquid-nitrogen-cooled sample tube and put into the cavity. It has been proven that during this irradiation procedure the temperature of the powder stays well below 120 K.

The X-band EPR and ENDOR measurements were performed on a Bruker ESP300E spectrometer with ENDOR/Triple extension, equipped with an Oxford ESR10 flow cryostat. The Q-band spectra were measured with a Bruker Elexsys E500 spectrometer, equipped with an Oxford CF935 cryostat.

3. Experimental results

3.1. EPR results

3.1.1. $T < 170$ K. Prior to irradiation and after irradiation at room temperature, no iridium-related EPR signals were detected. When the EPR spectra before and after x-ray irradiation at low temperature ($T < 120$ K) are compared, the formation of a spectrum related to Ir^{2+} centres is observed. The X-band EPR spectrum after irradiation consists mainly of two parts corresponding to $g_\perp$ and $g_\parallel$ respectively (figure 1). The spectrum was recorded at 20 K ($\nu = 9.53$ GHz) and is typical for Ir^{2+} as mentioned above and as will be further substantiated below. The $g_\perp$-component of the spectrum is better resolved than the $g_\parallel$-part, and we will confine ourselves to the study of the former. The EPR spectrum formed at low temperature ($T < 120$ K) will be labelled as LTir. For such an Ir^{2+} $5d^7$ low-spin complex, the unpaired electron is mainly localized in a d_{z^2} orbital and strongly interacts with two equivalent nearest-neighbour chlorine ions. Consequently the EPR spectra are interpreted by considering the

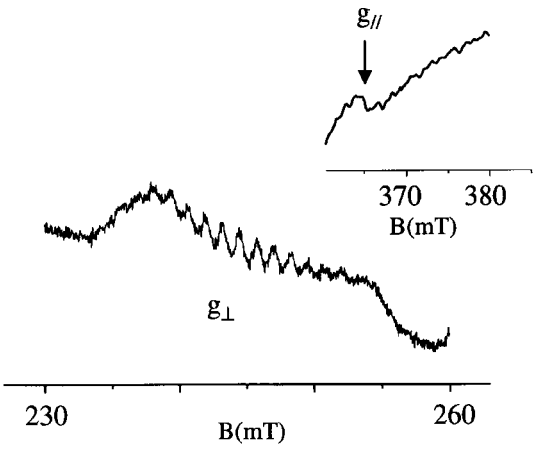

Figure 1. The EPR spectrum at 20 K of the Ir^{2+} complex in AgCl powder after x-ray irradiation at low temperature ($T < 120$ K).

interaction of the unpaired electron with the central Ir nucleus ($I = 3/2$ for $^{191/193}$Ir), splitting the EPR resonance into four, and the two equivalent Cl nuclei ($I = 3/2$ for $^{35/37}$Cl), causing an additional splitting of each hyperfine component into seven lines.

When zooming in around $g_\perp$ and comparing the X- and Q-band EPR spectra (figure 2(a)), we observed that the Q-band spectrum is broader than the corresponding X-band spectrum. This could be attributed to either the orthorhombicity of the g-tensor or to the presence of two defects with slightly different g-values. For the moment the former will be assumed and this will be substantiated below. For the powder EPR simulations the program SimFonia (WinEPR, Version 1.25 from Bruker) was used. Both X- and Q-band spectra could be convincingly simulated using the same set of spin Hamiltonian parameters, reported in table 1. The data are compared with the single-crystal data for AgX:Ir^{2+} [10] and on NaCl:Ir^{2+} [12, 13].

Table 1. EPR parameters for Ir^{2+} complexes in AgCl photographic emulsions and NaCl, AgCl and AgBr single crystals (hyperfine values in MHz). The subscripts indicate the error in the last digit.

	g_x	g_y	g_z	$A_\perp^{Ir}$	$A_\parallel^{Ir}$	$A_\perp^{Cl\,or\,Br}$	$A_\parallel^{Cl\,or\,Br}$	Reference
Ir^{2+}: single crystal								
AgCl	2.77_2	2.77_2	1.88_3	198	122	50	96	[10]
AgBr	2.69_2	2.69_2	1.91_9	186	112.8	249.9		[10]
Ir^{2+}: microcrystals								
AgCl: LTir	2.773_5	2.751_5	1.88_3	190_4	—	48_1	—	This
AgCl: HTir	2.758_2	2.758_2	1.88_3	190_4	—	48_1	—	work
Ir^{2+} in NaCl (melt-grown)	2.868_1	2.868_1	1.866_1	247	145	36	84	[13]
Ir^{2+} in NaCl (solution grown):								
Species A	2.813	2.813	1.904	189	111	36	81	[12]
Species B	2.866	2.866	1.867	243	153	36	81	[12]

3.1.2. $T > 170$ K. After a thermal pulse anneal of the low-temperature x-ray-irradiated powder (the powder was heated to a temperature above 170 K for typically ten minutes and then cooled down to the optimum measuring temperature of 20 K) the spectrum has slightly changed (figure 2(b)): the Q-band spectrum is narrower than that for $T < 170$ K and the (super)hyperfine structure, both in X- and Q-band, is much better resolved. Again the

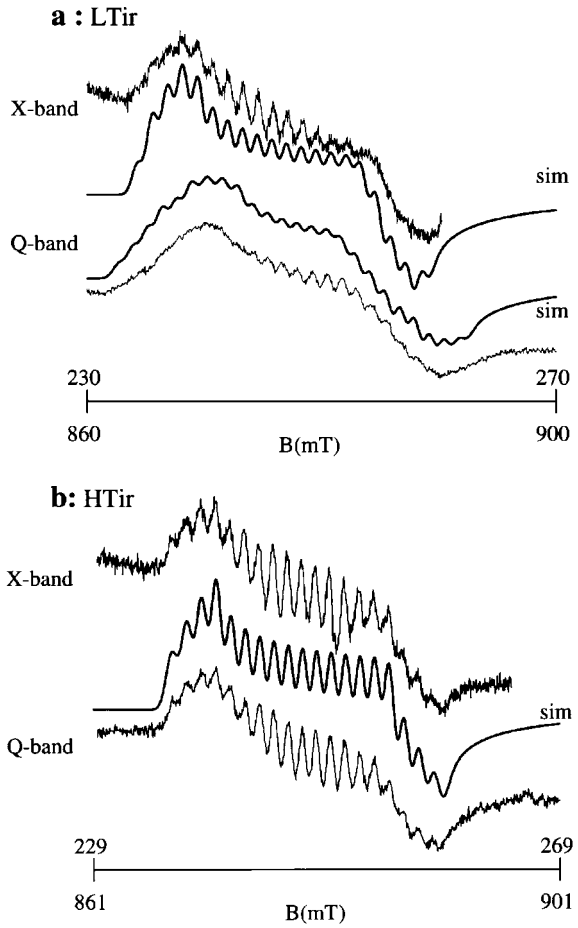

Figure 2. The low-field parts of the X-band ($\nu = 9.53$ GHz) and Q-band ($\nu = 34$ GHz) EPR spectra of the two Ir^{2+} complexes observed in AgCl photographic emulsions at 20 K. The data used for the simulations are shown in table 1. (a) The complex formed upon x-ray irradiation at low temperature ($T < 120$ K): LTir. (b) The complex formed upon x-ray irradiation at low temperature ($T < 120$ K) and pulse annealing at 170 K: HTir.

spectrum can be interpreted as the result of the interaction of the unpaired electron with the central Ir nucleus and two axial chlorine nuclei. When the X- and Q-band spectra are compared (figure 2(b)), we observe that they have identical structure. This points to axial symmetry and non-composite character for the spectrum. This high-temperature centre will be labelled HTir. Both X- and Q-band spectra could be convincingly simulated again using the data in table 1.

3.2. ENDOR results

A powder EPR spectrum is the superposition of single-crystal EPR spectra for all orientations. Therefore a lot of angle-dependent information is averaged out. An ENDOR spectrum is the result of the change of the intensity of a partially saturated EPR resonance as a function of the frequency of an incident radio-frequency (RF) signal. For a certain magnetic field within the EPR powder envelope, only those microcrystal orientations for which the EPR spectrum

is saturated will contribute to the ENDOR spectrum. In this way angle-dependent information can be obtained by setting the magnetic field to several positions within the powder envelope. This is known as the orientation-selection principle [14].

The ENDOR spectrum of each nucleus is interpreted using the second-order solutions of the usual spin Hamiltonian

$$\hat{H}_S = \beta \vec{B} \cdot \overleftrightarrow{g} \cdot \hat{\vec{S}} + \hat{\vec{S}} \cdot \overleftrightarrow{A}^{\mathrm{i}} \cdot \hat{\vec{I}}^{\mathrm{i}} - g_N^{\mathrm{i}} \beta_N \vec{B} \cdot \hat{\vec{I}}^{\mathrm{i}} + \hat{\vec{I}}^{\mathrm{i}} \cdot \overleftrightarrow{Q}^{\mathrm{i}} \cdot \hat{\vec{I}}^{\mathrm{i}}$$

with i = ^{107}Ag, ^{109}Ag, ^{35}Cl or ^{37}Cl.

The quadrupole interaction only has to be taken into account for the chlorine nuclei ($I > 1/2$).

In figure 3 the X- and Q-band ENDOR spectra, taken at 20 K, are shown. The spectra were recorded with the magnetic field set in the centre of the EPR envelope of figures 2(a)

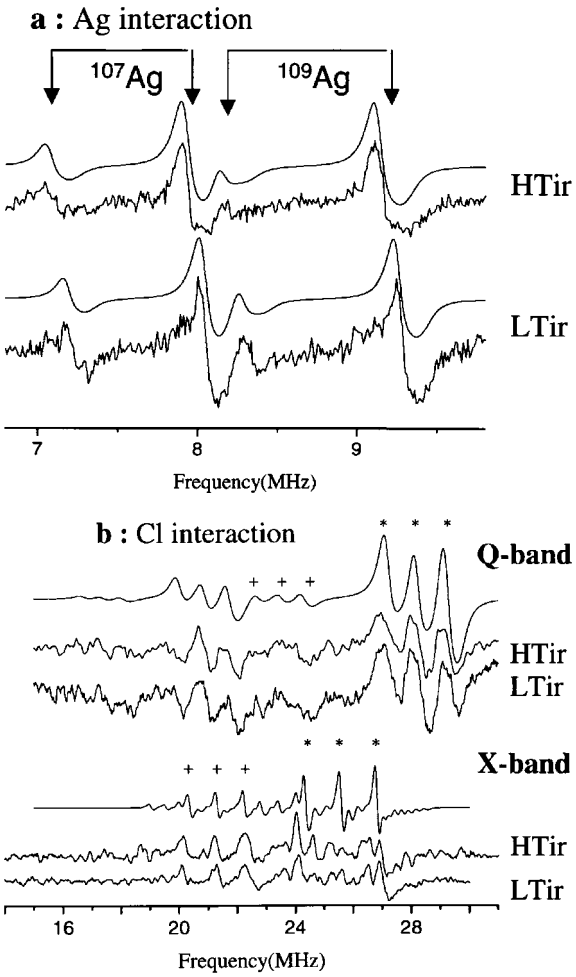

Figure 3. X- and Q-band ENDOR spectra recorded at 20 K and at $g = g_\perp$ for HTir and $g = (g_x + g_y)/2$ for LTir. The data extracted from the simulations are given in table 2. (a) A small but significant difference can be observed between the axial Ag interactions for LTir and HTir. (b) No difference is observed between the Cl interactions of LTir and HTir. The $M_s = -1/2$ transitions of the ^{35}Cl nuclei and the ^{37}Cl nuclei are marked with $*$ and + respectively.

Table 2. ENDOR data (in MHz) for the LTir and HTir Ir^{2+} complexes in the photographic AgCl emulsion (A- and Q-tensor principal axes are assumed coincident with the g-tensor principal axes).

Centre	Nucleus	$A_\perp$	$Q_\perp$
LTir	^{35}Cl(ax)	49.0_3	0.31_2
	^{109}Ag(ax)	-17.52_5	—
HTir	^{35}Cl(ax)	49.0_3	0.31_2
	^{109}Ag(ax)	-17.27_5	—

and 2(b). The intensity of the ENDOR spectrum strongly decreases when moving away from this position. For LTir this position corresponds to $g = (g_x + g_y)/2$ and for HTir to $g = g_\perp$. Because of the very small orthorhombic distortion of the LTir complex the EPR spectra of the g_x- and g_y-components overlap almost completely. Consequently the ENDOR spectra of LTir (at $g = (g_x + g_y)/2$) contain contributions from both the g_x- and the g_y-components. The most intense resonances were assigned to interactions of the unpaired electron with two equivalent Ag (figure 3(a)) and two equivalent Cl nuclei (figure 3(b)) along the $g_\parallel$-axis of the complex (axial Ag and Cl) (figures 4(a), 4(b)).

The ENDOR spectra were simulated using an adapted version of a program described earlier [15] to take into account the resolved hyperfine and superhyperfine structure in the EPR spectrum [7]. In spite of the overlap of the g_x- and g_y-components for LTir, the ENDOR spectra in figure 3 could be convincingly simulated using axial hyperfine and quadrupole tensors for both LTir and HTir for the Ag ($I = 1/2$ for ^{107}Ag and ^{109}Ag) and Cl ($I = 3/2$ for ^{35}Cl and ^{37}Cl) nuclei. The orthorhombic distortion for LTir could not be detected using ENDOR. There is an intensity ratio of approximately 3/1 observed for the $M_s = -1/2$ and $M_s = 1/2$ transitions (in agreement with [8, 9]) which was taken into account for the simulations. The values of the Ag and Cl tensors extracted from these simulations are given in table 2. They are in agreement with the EPR data (table 1) and are of the same order of magnitude as the data for Rh^{2+} centres in AgCl and NaCl (table 3). For both interactions the principal axes of the tensors are assumed to be along the crystal axes. In the Q-band the ENDOR interactions of the axial Ag nuclei could not be detected. The intensity of the Ag interactions is in the X-band lower than for the Cl interactions, and because in the Q-band the intensities of the ENDOR

Table 3. EPR and ENDOR parameters for Rh^{2+} complexes in AgCl photographic emulsions and NaCl single crystals (hyperfine values in MHz). The subscripts indicate the error in the last digit. These superhyperfine tensors were determined with ENDOR. For the present study only the A_x- and A_y-values are relevant. The principal axes are along ⟨100⟩, ⟨010⟩ and ⟨001⟩.

	g_x	g_y	g_z	A_x^{Cl}	A_y^{Cl}	$A_x^{Ag\text{ or }Na}$	$A_y^{Ag\text{ or }Na}$	Reference
Rh^{2+} in NaCl								
O(I)[(a)]	2.4797_4	2.4712_4	2.0118_8	33.9_1	33.9_1	3.31_3	3.31_3	[21, 22]
O(II)	2.4779_4	2.4301_4	2.0154_4	34.0_2	34.1_2	3.15_3	3.17_3	[21, 26]
RTAX	2.4510_1	2.4510_1	2.0190_8	33.9_1	33.9_1	2.88_3	2.88_3	[21, 23]
Rh^{2+} in AgCl								
R4	2.5355_{10}	2.5355_{10}	2.011_5	37.8_5	36.2_2	-12.78_3	-12.78_3	[8]
R5	2.480_2	2.431_2	2.011_5	38.5_2	38.7_2	-11.47_3	-11.47_3	[8]
R6′	2.426_1	2.395_1	2.011_1	39.1_2	39.1_2	-9.8_1	-9.8_1	[8]
R6	2.4091_5	2.4091_5	2.011_5	39.2_2	39.2_2	—	—	[8]

[(a)] The principal axes of the g-tensor are along ⟨110⟩, ⟨$\bar{1}$10⟩ and ⟨001⟩.

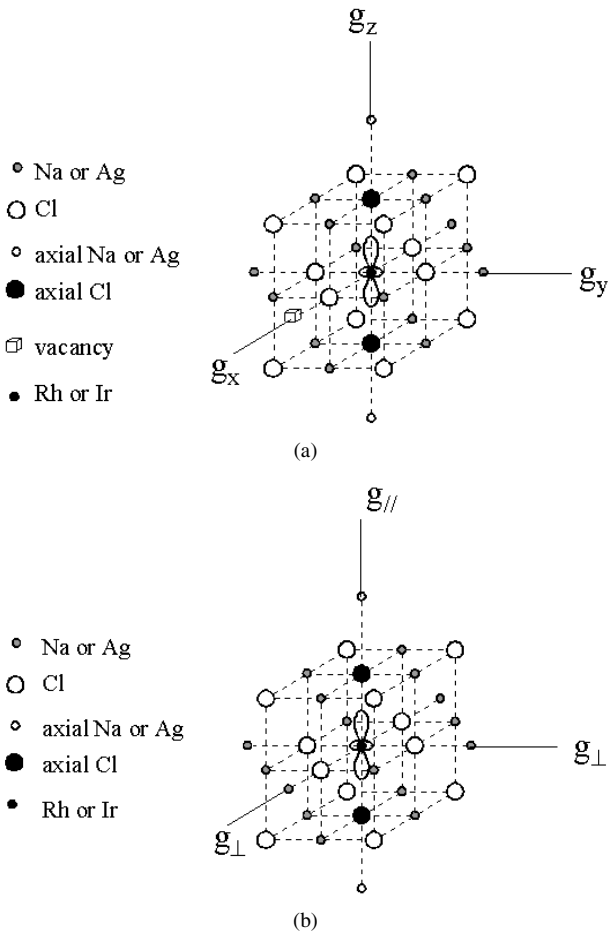

Figure 4. Microscopic models for possible $[MCl_6]^{4-}$ complexes in NaCl or AgCl (M = Rh or Ir). Vacancies are found in next-nearest-neighbour positions. (a) The model for O(II), R6′ and LTir [26, 8]. (b) The model for RTAX, R6 and HTir [23, 8].

signals are lower compared to those for the X-band, no Ag ENDOR interactions are observed in the Q-band.

The values of the Cl tensor were determined from the Q-band ENDOR spectra. The axial Cl interactions are identical for the two centres within experimental error. On the other hand, there is a small but significant difference between the axial Ag interactions of the two complexes. A clear shift towards lower frequencies is detected when LTir is converted into HTir (figure 3(a), table 2). Whereas the EPR spectra for $T < 170$ K suggest the possibility of a second centre, the ENDOR spectrum for $T < 170$ K points to only one dominant centre. The presence of e.g. HTir for $T < 170$ K could account for the very weak shoulders in the ENDOR spectrum. However, because LTir and HTir are strongly related centres it is believed that the EPR spectrum for $T < 170$ K is, accordingly, completely dominated by LTir.

The correspondence between the simulation and the observed spectra of the ^{35}Cl interaction in the X-band (figure 3(b)) is rather poor. This is attributed to additional splittings of the ENDOR lines, which were not taken into account in the simulations. These splittings were also observed for the X-band ENDOR transitions of the axial ^{35}Cl nuclei for $[RhCl_6]^{4-}$ complexes

in NaCl and AgCl [16, 17]. They have been attributed to indirect spin–spin coupling [18] between equivalent chlorine ions, i.e. ^{35}Cl–^{35}Cl and ^{37}Cl–^{37}Cl pairs. The splittings due to an indirect coupling between inequivalent chlorine ions, ^{35}Cl–^{37}Cl pairs, are smaller than the linewidth and thus not resolved. The chlorine isotope pairs ^{35}Cl–^{35}Cl, ^{35}Cl–^{37}Cl and ^{37}Cl–^{37}Cl occur in the approximate ratio 9:6:1 (natural abundance of ^{35}Cl: 75.77% and of ^{37}Cl: 24.23%). Therefore the largest contribution to the ENDOR spectrum is due to the ^{35}Cl–^{35}Cl pairs. The ENDOR transitions of the ^{37}Cl–^{37}Cl pairs and the transitions of ^{35}Cl–^{37}Cl pairs are totally superimposed [16, 17]. This second-order effect is reduced at higher microwave frequencies (almost not observed in the Q-band).

For both centres, LTir and HTir, we could detect the ENDOR interaction from neither the central Ir nucleus nor the protons.

4. Discussion

The EPR and ENDOR data determined (tables 1 and 2) for both LTir and HTir are consistent with a d^7 low-spin-state system in which the odd electron is localized mainly in a $5d_{z^2}$ orbital of an octahedral complex [19]. The only possible alternative for a photoproduced centre would be an Ir^{4+} complex, a hole-trapped species, but the data (table 1) are not compatible with such an assignment [10]. The most reasonable ordering for the d-orbital energies for a d_{z^2} ground state is $d_{xz} = d_{yz} < d_{xy} < d_{z^2} < d_{x^2-y^2}$, and both complexes are tetragonally elongated along the molecular z-axis (figures 4(a), 4(b)). Consequently both centres have near to axial symmetry and, besides the interaction with the central Ir nucleus, the interaction with the axial Cl nuclei dominates the EPR spectrum, although the Cl nuclei in the equatorial plane are closer to the Ir nucleus.

Before x-ray irradiation of the photographic emulsion, no detectable EPR signals are present. This means that the iridium is incorporated in diamagnetic form, i.e. Ir^{3+}. After x-ray irradiation at low temperature, the complex traps an electron and Ir^{2+} is left, which can be detected using EPR. From the comparison of the X- and Q-band EPR spectra of LTir, we conclude that the complex has a small orthorhombic distortion. However, from the available EPR and ENDOR spectra it is not possible to determine the exact symmetry of the defect: orthorhombic-I (principal axes of the g-tensor along [110], [1$\bar{1}$0] and [001]) or orthorhombic-II (principal axes of the g-tensor along [100], [010] and [001]). After a pulse anneal to $T > 170$ K, it was concluded from the comparison of the X- and Q-band data for HTir that the HTir spectrum has axial symmetry and is not composite. For axial defects in the cubic AgCl lattice the symmetry can be trigonal or tetragonal, but trigonal symmetry can be ruled out because of the strong interaction of the unpaired electron with the Cl and Ag nuclei along the $g_{\|}$-axis. The ENDOR spectrum of the axial Ag nuclei for $T < 170$ K is dominated by LTir and for $T > 170$ K the spectrum is not composite indicating that only HTir is present. These Ag ENDOR interactions indicate that the temperature treatment completely converts the LTir defect into the HTir defect. The EPR parameters of HTir are within experimental error identical to the values reported for the axial $[IrCl_6]^{4-}$ defect in AgCl by Eachus and Graves [10]. We assumed that the two defects are identical.

Dependent on the preparation conditions, four different Rh^{2+} complexes have been detected in Rh-doped AgCl microcrystals [8]. These centres have been proposed to be $[RhCl_4X_2]^{(4-2y)-}$ (labelled R4, orthorhombic-I symmetry), $[RhCl_5X]^{(4-y)-}$ (R5, orthorhombic-II symmetry) with $y = 0$ if X = OH^- and $y = 1$ if X = H_2O [8]; and two non-aquated centres: $[RhCl_6]^{4-}\cdot$1Vac (one vacancy, labelled R6′, orthorhombic-II symmetry, figure 4(a)) and $[RhCl_6]^{4-}\cdot$0Vac (no vacancies, R6, axial symmetry, figure 4(b)) [8]. After x-ray irradiation at room temperature the non-fully charge compensated R6 complex (axial

symmetry) is more stable than the fully charge compensated R6′ complex. All vacancies are in next-nearest-neighbour positions and no other vacancy configurations are observed. When the number of aquated ligands decreases, the absolute values of A_x and A_y for the axial Cl interaction increase (table 3) and the average of g_x and g_y decreases significantly. However, the A_x- and A_y-values of the axial Cl interaction and the average of g_x and g_y do not change when only the number of vacancies changes (comparison of R6 and R6′). This is exactly what is observed for LTir and HTir (tables 1 and 3) and we conclude that the conversion from LTir into HTir is correlated with vacancy movement and not with changes in the ligand structure of the complex. Because the HTir complex is also observed in melt-grown crystals, where no aquation is expected, and because no interactions with nearby protons are observed, we conclude that HTir and LTir are both $[IrCl_6]^{4-}$ complexes. The HTir defect has the same symmetry as the R6 complex and it is assumed that the models for the two defects are identical (figure 4(b)).

The fact that the conversion from LTir into HTir is indeed correlated with vacancy movement is further supported by the study of $[RhCl_6]^{4-}$ complexes in solution-grown NaCl single crystals on which similar pulse-anneal experiments have been reported [20, 21]. When the NaCl single crystals are x-ray irradiated at 77 K, only one $[RhCl_6]^{4-}$ complex is observed with orthorhombic-I symmetry, called O(I), charge compensated with two vacancies [22]. When the crystals are pulse annealed to $T > 180$ K, one of the vacancies migrates and a fully charge-compensated defect is left, labelled O(II), having orthorhombic-II symmetry [20] (figure 4(a)). This conversion is not complete and a certain equilibrium is reached between O(I) and O(II) defects [21]. Finally, when the crystals are pulse annealed to room temperature both O(I) and O(II) convert into a third $[RhCl_6]^{4-}$ complex, which is not charge compensated and which is labelled RTAX [23] (figure 4(b); axial symmetry). We want to stress that the not fully charge compensated RTAX (axial symmetry) complex is stable at room temperature. For these complexes all vacancies are in next-nearest-neighbour cation positions and there were no complexes detected with other vacancy configurations. Because the X-band EPR spectra of these three defects strongly overlap, just as for LTir and HTir, this conversion and the equilibrium between the three different defects, as a function of the pulse-anneal temperature, were monitored using X-band ENDOR [20]. It is a conclusion from this study that the x- and y-components of the superhyperfine tensor (A_x and A_y) of the axial Cl nuclei do not change significantly (see R6 and R6′) and that those of the axial Na nuclei decrease when the number of charge-compensating vacancies decreases (table 3). A similar decrease of the absolute value of the axial Ag interaction is seen for the conversion of LTir into HTir. The differences in g-values for these three Rh complexes are comparable with the differences observed for LTir and HTir (tables 1 and 3). The conclusion is that the conversion from LTir into HTir is indeed the result of the migration of one or more charge-compensating vacancies away from the complex.

Marchetti and Eachus [11] report on an Ir^{3+} complex in AgBr photographic emulsions. They propose that the Ir^{3+} is incorporated as $[IrCl_6]^{3-}$ charge compensated with two vacancies ($[IrCl_6]^{3-}\cdot 2$Vac). After irradiation at $T < 70$ K the centre traps an electron and becomes paramagnetic, and they suggest that the complex remains charge compensated by the two vacancies. Between 70 K and 100 K a substantial fraction of the centres thermally ionize and it is proposed that finally vacancy motion generates the more stable, neutral centres $[IrCl_6]^{4-}\cdot 1$Vac. At room temperature the lifetime of the trapped electrons for the $[IrCl_6]^{4-}$ defects in AgBr is very small ($\approx$20 ms) and the paramagnetic centres decay by several competitive pathways, one involving the reduction of an interstitial silver ion to produce the nucleus of a latent image centre at an adjacent site. The Ir^{3+} trap is reset and can trap a second electron. However, if we want to use the above conclusions we have to take into account

the following two differences between AgBr and AgCl. Marchetti and Eachus report that the lifetime for $[IrCl_6]^{4-}$ complexes in AgCl (several seconds) is many orders larger than in AgBr. This can however be ignored because the lifetime is still too small to observe any EPR signals after x-ray irradiation at room temperature. All trapped electrons are lost before the sample is cooled to a sufficiently low temperature. A second difference is in the temperature at which Ag^+ vacancies become mobile. Several studies report that the Ag^+ vacancies in AgCl become mobile between 100 and 130 K [24, 25]. This is significantly different from the case for AgBr and is reflected in the proposed model for LTir.

Taking into account the latter studies [11, 24, 25], the study of Rh^{2+} in NaCl and AgCl and the symmetry of HTir, we propose that LTir has one charge-compensating vacancy in a next-nearest-neighbour position (figure 4(a)) and that HTir has none (figure 4(b)). Both models are in agreement with the non-composite character of both spectra ($T < 170$ K and $T > 170$ K), the orthorhombic symmetry for LTir and the axial symmetry for HTir. Completely in agreement with the study of Marchetti and Eachus, we propose the following sequence of reactions:

- Shallow trapping:

$$([IrCl_6]^{3-}\cdot 2Vac)^0 + e^- \rightarrow ([IrCl_6]^{3-}\cdot 2Vac\cdot e^-)^{1-}.$$

- Electronic relaxation:

$$([IrCl_6]^{3-}\cdot 2Vac\cdot e^-)^{1-} \rightarrow ([IrCl_6]^{4-}\cdot 2Vac)^{1-}.$$

- Ionic relaxation:

$$([IrCl_6]^{4-}\cdot 2Vac)^{1-} \rightarrow ([IrCl_6]^{4-}\cdot 1Vac)^0 + [Vac_{free}]^{1-}.$$

- Migration:

$$([IrCl_6]^{4-}\cdot 1Vac)^0 \rightarrow ([IrCl_6]^{4-}\cdot 0Vac)^{1+} + [Vac_{free}]^{1-}.$$

The first three sequences occur during x-ray irradiation ($T < 120$ K), while the last process occurs when the temperature is increased to $T > 170$ K.

5. Conclusions

A combined X- and Q-band EPR and ENDOR study on x-ray irradiated AgCl powders doped with iridium has revealed the presence of two different $[IrCl_6]^{4-}$ complexes. The first defect is formed after x-ray irradiation at low temperature ($T < 120$ K) and has orthorhombic symmetry. It is proposed that the complex is charge compensated by one vacancy in a next-nearest-neighbour position. When this AgCl powder is then subjected to a pulse anneal at $T > 170$ K, the orthorhombic complex is completely converted into a second $[IrCl_6]^{4-}$ complex which has axial symmetry. For the latter defect a non-charge-compensated model is proposed.

Acknowledgments

The authors would like to acknowledge the Fonds voor Wetenschappelijke Onderzoek (FWO, Flanders, Belgium), the Vlaams Instituut voor de Bevordering van het Wetenschappelijk Technologisch Onderzoek in de Industrie (IWT, Flanders, Belgium), and Agfa-Gevaert N.V. for financial support. K Sabbe is financially supported by the 'Flemish Institute for the Encouragement of Scientific and Technological Research in the Industry (IWT)'.

References

[1] Eachus R S and Olm M T 1991 *J. Soc. Photogr. Sci. Technol. Japan* **54** 294
[2] Vercammen H, Ceulemans T, Schoemaker D, Moens P and Vandenbroucke D 1996 *Proc. IS&T 49th Annual Conf. (Minneapolis, MN, May 1996)* p 54
[3] Vercammen H, Ceulemans T, Schoemaker D, Callens F and Vandenbroucke D 1998 *J. Appl. Phys.* **84** 4414
[4] Moens P, Vercammen H, Vandenbroucke D, Callens F and Schoemaker D 1996 *Proc. IS&T 49th Annual Conf. (Minneapolis, MN, May 1996)* p 56
[5] Schweizer S and Spaeth J M 1997 *J. Phys. Chem. Solids* **58** 859
[6] Vrielinck H, Sabbe K, Callens F, Matthys P, Vercammen H, Schoemaker D and Vandenbroucke D 1998 *Proc. ICPS Conf. (Antwerp, Belgium, September 1998)* p 80
[7] Vrielinck H, Callens F, Matthys P and Vandenbroucke D 1999 *Solid State Commun.* **110** 87
[8] Vrielinck H, Sabbe K, Callens F, Matthys P and Vandenbroucke D 2000 *Spectrochim. Acta* A **56** 319
[9] Pawlik T D, Eachus R S, McDugle W G and Baetzold R C 1998 *J. Phys.: Condens. Matter* **10** 11 795
[10] Eachus R S and Graves R E 1976 *J. Chem. Phys.* **65** 1530
[11] Marchetti A P and Eachus R S 1992 *Adv. Photochem.* **17** 145
[12] Vugman N V and Pinhal N M 1979 *Mol. Phys.* **38** 1999
[13] Zdravkova M, Sabbe K, Callens F, Dobbeleir E and Matthys P 1999 *Imag. Sci. J.* **47** 63
[14] Rist G H and Hyde J S 1968 *J. Chem. Phys.* **49** 2449
[15] Van Doorselaer S, Callens F, Maes F and Boesman E 1995 *Phys. Rev.* B **51** 12 480
[16] Olm M T, Niklas J R, Spaeth J M and Symons M C R 1998 *Phys. Rev.* B **38** 4343
[17] Schweizer S and Spaeth J M 1997 *J. Phys. Chem. Solids* **58** 859
[18] Chung N S and Mieher R L 1975 *Phys. Rev.* B **12** 4755
[19] Abragam A and Bleaney B 1970 *Electron Paramagnetic Resonance of Transition Ions* (Oxford: Clarendon)
[20] Sabbe K, Vrielinck H, Callens F, Boesman E, Vercammen H, Käß H, Goovaerts E, Bouwen A and Schoemaker D 1998 *J. Chem. Soc. Faraday Trans.* **94** 2993
[21] Vercammen H, Schoemaker D, Käß H, Goovaerts E, Bouwen A and Vrielinck H 1998 *J. Appl. Phys.* **84** 428
[22] Callens F, Vrielinck H, Matthys P, Zdravkova M, Vercammen H and Schoemaker D 1998 *J. Appl. Phys.* **84** 422
[23] Zdravkova M, Vrielinck H, Callens F, Boesman E, Vercammen H and Schoemaker D 1997 *J. Appl. Phys.* **82** 2476
[24] Van Robbroeck L 1985 *PhD Thesis* University of Antwerp
[25] Olm M T, Eachus R S and McDugle W G 1993 *Bulg. Chem. Commun.* **26** 350
[26] Sabbe K, Callens F and Boesman E 1998 *Appl. Magn. Reson.* **15** 539